

An Analytical System for Single Nanomaterials: Combination of Capillary Electrophoresis with Raman Spectrometry or with Scanning Probe Microscopy for Individual Single-Walled Carbon Nanotube Analysis

*Tatsuhiko Yamamoto,¹ Yoichi Murakami,² Jin Motoyanagi,³
Takanori Fukushima,⁴ Shigeo Maruyama,⁵ and Masaru Kato^{1, 6*}*

¹ Center for NanoBio Integration, The University of Tokyo, Tokyo 113-8656, Japan

² Department of Chemical System Engineering, Graduate School of Engineering,
The University of Tokyo, Tokyo 113-8656, Japan

³ ERATO-SORST Aida Nanospace Project, Japan Science and Technology Agency,
National Museum of Emerging Science and Innovation, Tokyo 135-0064, Japan

⁴ Functional Soft Matter Engineering Laboratory, Advanced Science Institute,
RIKEN, Saitama 351-0198, Japan,

⁵ Department of Mechanical Engineering, Graduate School of Engineering,
The University of Tokyo, Tokyo 113-8656, Japan

⁶ Graduate School of Pharmaceutical Sciences and Global COE Program,
The University of Tokyo, Tokyo 113-0033, Japan

* To whom corresponding should be addressed: E-mail: kato@cnbi.t.u-tokyo.ac.jp

ABSTRACT

Nanomaterials continue to attract widespread attention in many scientific and technological fields. The sizes and shapes of nanomaterials determine their physical and chemical properties. We develop an analytical system for single nanomaterials that combined capillary electrophoresis (CE) with high sensitive detection method. In this manuscript, we hyphenated CE with Raman spectrometry or with scanning probe microscopy (SPM) for the analysis of individual single-walled carbon nanotubes (SWNTs). To combine CE with these detection techniques, we fabricated a fraction collection system that can collect droplets of small volume (less than 300 nL) in a small hydrophilic spot on a fractionation glass plate. The CE-separated fractions were concentrated by the evaporation of effluent, thus increasing the sensitivity by more than a factor of ten in case of Raman spectrometric analysis. We characterized the fractionated SWNTs by means of Raman spectrometry and SPM, both of which detected single SWNTs. Raman analysis enabled to recognize the diameter difference of SWNTs only 0.02 nm and it was supposed that the separation by CE occurred on the basis of the SWNTs' diameters. We also observed a fibrous SWNT structure of 1 nm height by SPM, and this structure was thought to be a single SWNT. These hyphenated analytical systems enable the precise separation and characterization of individual SWNTs. We expect that methods developed herein can be applied to the analysis of many nanomaterials, because these methods offer separation and analysis with nanometer-scale precision. The characterization of nanomaterials at the single-compound level will be a necessity as the field of nanomaterials continues to evolve, and these hyphenated methods may become indispensable techniques for the analysis of

widely available nanomaterials.

INTRODUCTION

The field of nanotechnology currently is expanding dramatically in many research fields, and many different kinds of nanoscale compounds have been developed recently.¹⁾ These nanomaterials receive much attention owing to their excellent functions, as well as their risk to the environment and health,²⁾ because it is believed that even a single nanostructure can cause the strong effects. For example, single quantum dots are now used as probes for single biomolecules, and single nanowires are used for integrated electrically driven photonic devices.³⁻⁶⁾ Therefore, the demand for an efficient and accurate method for single-compound analysis of these nanomaterials is increasing.

Such evaluation of single nanomaterials can be made possible through the improvement of currently used analytical techniques or instruments. Analysis of single nanotubes, nanoparticles, and nanowires by means of probe and electron microscopies, dynamic light scattering, and Raman spectrometry has been reported.^{7,8)} However, few studies have examined separation techniques for nanomaterials. Capillary electrophoresis (CE) is a highly efficient separation technique, and many compounds, such as chiral compounds, antibodies, and nucleic acids, are separated well by means of CE.⁹⁻¹¹⁾ We hypothesized that efficient separation by means of CE coupled with a highly sensitive detection method such as Raman spectrometry or scanning probe microscopy (SPM) could be suitable for the analysis of nanomaterials. CE and detection techniques can be coupled in either an on-line or off-line configuration.¹²⁾ The on-line configuration is more suitable for automation; however, it is fundamentally impossible to develop an on-line SPM system, because the movement of analytes must be suppressed during SPM analysis if nanometer

resolution is to be achieved. Off-line coupling of CE to a detection instrument represents an alternative to the on-line configuration and offers increased flexibility for independent optimization of the CE and detection methods, making the majority of the CE fractions available for further characterization. Several previously reported off-line methods have involved fraction collection in vials¹³⁻¹⁵⁾ or elution onto the fraction plate by a larger coaxial sheath flow.¹⁶⁻²²⁾ Though effective, these fraction-collection methods are somewhat problematic because detecting nanomaterials in the fractions can be difficult, owing to substantial dilution caused by the addition of large volumes of supplemental fluid to the CE effluent.

DNA is a suitable analyte for separation by CE, and the innovation of sequencing technology based on CE contributed greatly to the success of the human genome project.^{23,}
²⁴⁾ DNA is a nanomaterial with a fibrous structure. Therefore, we expected that other nanomaterials with similar fibrous structures could be separated by CE. Recently, many nanoscale fibrous compounds including β -amyloid and carbon nanotubes have received considerable attention. We have reported an efficient separation method for β -amyloid using CE and have shown the effectiveness of this method for the screening of potential therapeutic agents for Alzheimer's disease.²⁵⁾ Although this method separates β -amyloid rapidly, we have not yet identified each peak in the resulting electropherograms, because the aggregation reaction of β -amyloid is very rapid, causing the structures to change dramatically depending on time.²⁶⁾ Single-walled carbon nanotubes (SWNTs) are also fibrous nanomaterials and have novel properties that make them potentially useful in many applications in nanotechnology, electronics, optics, and other fields.²⁷⁻²⁹⁾ SWNTs exhibit

extraordinary strength and unique electrical properties and are efficient conductors of heat. Although these properties of SWNTs were changed by their structure and there are various attempts have been done to obtain SWNTs with defined chiral indices and diameters by means of the selective production or separation that include separation by CE,³⁰⁻³⁴⁾ no effective methods have been reported.³⁵⁾ We have developed a method for preparing individually dispersed SWNTs using a triphenylene derivative as a dispersant.³⁶⁾ The individually dispersed SWNTs are stable in solution and remain individually dispersed even after drying.³⁷⁾ Therefore, SWNTs were used as analytes in this study.

In this study, we fabricated a new fractionation system that enriched sample concentration in individual fractions, and we also developed an analytical system consisting of CE hyphenated with either Raman spectrometry or SPM for the analysis of SWNTs. The size and shape of fractionated SWNTs were characterized by means of the developed systems. We found that these two CE-coupled techniques were powerful for the detection and characterization of single SWNTs.

EXPERIMENTAL

Materials and Chemicals

Purified HiPco was supplied from Rice University. The dispersant of SWNTs, 2,3,6,7,10,11-hexakis (carboxydecyloxy) triphenylene, was synthesized as reported previously.³⁶⁾ Glycine and sodium hydroxide were purchased from Kanto Chemical Co., Inc. (Tokyo, Japan). Ammonium acetate was purchased from Wako Pure Chemical Industries, Ltd. (Osaka, Japan). Deuterium oxide was purchased from Sigma-Aldrich Japan K.K. (Tokyo, Japan). Two types of slide glasses (Matsunami Glass Industry, Ltd, Osaka, Japan) were used as fraction plates. One type was non-coated, and the other was partially coated with a hydrophobic layer. The coated glass slide contained 570 hydrophilic spots in a 15 x 38 array, as shown Fig. 1. Each hydrophilic spot was 1 mm in diameter.

Sample preparation

The preparation of SWNTs dispersion was performed using bath sonicator (Branson model 5510) as reported previously.³⁶⁾ Finally, 1.0 mg of SWNTs was dispersed in 6 mL of 0.2 % (w/v) of dispersant D₂O solution. The SWNTs dispersion was ultracentrifuged for 1 h at 386,000 *g* with a Himac CS120GX centrifuge equipped with an S100AT6 angle rotor (Hitachi Koki, Tokyo, Japan). The supernatant was carefully collected and used in the experiments described here. The dispersed SWNTs could be stored for long periods of time, because the SWNTs and dispersant formed a stable complex in which SWNTs were individually dispersed in both liquid and dry states.³⁷⁾

Separation by CE.

All CE experiments were performed on a P/ACE System MDQ (Beckman Coulter, Inc., Fullerton, CA) with UV detection at 280 nm. Instrument operation and data collection were controlled by using the 32 Karat Software 8.0 package (Beckman Coulter, Inc.). The uncoated fused silica capillary (100- μ m i.d., 100-cm total length) from Polymicro Technologies Inc. (Phoenix, AZ) was used for separation. Solution of 100 mM Gly-NaOH buffer (pH 9) and 10 mM ammonium acetate (pH 9) were used as electrolyte for fractionation of Raman spectrometry and SPM samples, respectively. The injection of the sample was carried out by applying a pressure of 0.5 psi for 5 s. The separations were carried out at 30 kV with the anode at the sample injection end. For optimization of separation conditions, the UV detection window was placed 90 cm from the inlet vial, and the capillary outlet was placed in a vial containing electrolyte.

Fractionation

The location of the ultraviolet (UV) detector on the CE instrument did not permit simultaneous detection near the outlet of the capillary during fraction collection in our experimental setup. Therefore, for CE with fraction collection, a capillary with a UV detection window positioned 10 cm from the capillary inlet was used. The capillary outlet was positioned inside a fixed steel needle whose position was controlled by a robotic *x-y-z*-axis motion system (DiNa MaP, KYA-Technologies Corporation, Tokyo, Japan). The steel needle functioned as a cathode during the CE separations. A syringe pump (KDS100, Muromachi Kikai Co., Ltd., Tokyo, Japan) supplied the steel needle with a sheath flow

solution of MilliQ water. The rate of the sheath flow was 167 nL/min. Fractionated droplets of ~300-nL volume were collected.

Raman Spectrometry Analysis.

Raman spectra of SWNT were obtained using a Raman microscope (LabRAM HR-800 and LabRAM ARAMIS systems, HORIBA Jobin Yvon, Kyoto, Japan). In these systems, the Raman spectrometer is coupled to a microscope. Raman scattering was excited by a He-Ne laser at 633 nm. The laser beam was focused automatically on individual spots by means of a x 100/0.9 microscope objective to a spot of 1- μ m diameter. Accumulation time for one spectrum was mostly 10s. Spectra were recorded and processed (smoothing, baseline subtraction, and peak detection) by means of the LabSpec5 software (HORIBA Jobin Yvon).

SPM Analysis.

SPM measurements were conducted by using NanoWizard (JPK Instrument, Berlin, Germany) at room temperature. SWNT images were obtained in tapping mode using a commercial micro cantilever with a spring constant of 150 N/m (Olympus Corporation, Tokyo, Japan). SPM images were processed with JPK SPM image processing v.3 software.

Results and Discussion

Optimization of Fraction Conditions

Because the volume of effluent in CE is small (few hundreds to thousands of nanoliters), a substantial dilution of the separation zone occurred upon fractionation. This sample dilution caused difficulty for further analysis owing to the reduction or disappearance of signal. The dilution was mainly caused by the sheath liquid, which provides electrical contact with the outlet end of the separation capillary and increases the volume of droplets that are collected as fractions. The volume of fractionated droplets is influenced by many factors, but the distance between the end of capillary and the surface of the fraction plate is one of the most important factors. The volume of each droplet decreases with decreasing distance. Because the z -axis accuracy of the spotter we used in this study is good (0.1 mm), we could adjust the distance precisely. The hydrophobicity of the sheath liquid tube (Fig. 1c) was also important for the release of the droplet from the outlet end of the capillary. Therefore, a Teflon tube was used as the sheath liquid tube in this study. We set the distance between the end of the capillary and the fraction plate to about 0.5 mm, and the flow ratio of effluent and sheath flows was set at about 6:1. With these settings, droplets of ~300-nL volume were collected continuously. Furthermore, the dilution of the separation zone was small, because each fractionated droplet consisted mainly of the effluent, and the volume ratio of the eluent to sheath liquid was only 6:1.

We used a coated glass plate as a fraction plate to increase the concentration of fractionated SWNTs. The fractionated samples were automatically allocated on the 1-mm hydrophilic spots on this plate (see supporting movie). After drying, the spotted SWNTs

were effectively immobilized at the surface of the glass. These fractionated SWNTs were effectively concentrated prior to Raman spectrometry or SPM analysis, because during the drying process water evaporated and the enrichment of SWNTs occurred. This concentrated SWNT within the hydrophilic spots increased the probability of SWNTs being present within the measurement area of Raman spectrometry or SPM. In fact, use of the coated plate increased this probability by a factor of ~4. Furthermore, as stated above, in our fractionation system, the dilution of the separation zone by the sheath liquid was small, because the volume of the sheath liquid was one-sixth that of the fraction solution from CE. Therefore, the concentration of SWNTs on the fractionated plate was more than 3 times that in the CE separation column. If the size of the hydrophilic spots was decreased, the SWNT concentration would increase, thus facilitating easier characterization. A photograph and movie of the fractionation process are shown in Fig. 1 and in the supporting data, respectively.

Fractionated Sample Analysis by Raman Spectrometry (G-Band)

We applied the separation conditions used in our previous β -amyloid study to our present study with SWNTs,²⁵⁾ because β -amyloid also forms a fibrous structure. Figs. 2a and b show electropherograms of the dispersed solution of SWNTs and of the dispersant solution without SWNTs, respectively. A broad small peak was observed around 14 minutes in the solution with SWNTs, and a large peak was observed around 17 minutes in both solutions. The reproducibility of the relative migration times and peak height of former peak to EOF peak were satisfactory, and their RSDs were 1.12% and 2.25%, respectively,

which seem to indicate the acceptable reproducibility of our separation method. Although the similar electropherogram was obtained when analyzed a dispersed solution without ultracentrifugation, these reproducibility became wrong. The tangential mode (G^+ -band, 1590 cm^{-1}) of Raman spectrometry is a unique signal of SWNTs and is associated with carbon atom vibrations within the graphitic plane.⁷⁾ We fractionated the separation zone onto the glass plate every 15 seconds and measured the G-band of each fractionation to detect the presence of SWNTs. The results of these G-band measurements are shown in Fig. 2c. Although strong G-band signals were detected in the fractions corresponding to the small broad peak, no signal was obtained for those corresponding to the large peak. These results indicate that the former peak was derived from SWNTs and the latter one was derived from the dispersant. The migration time of the dispersant was slower than that of the SWNTs because the dispersant has six carboxyl groups per molecule, and the negative charge of these carboxyl groups caused electrophoretic movement toward the inlet side of the column. Because the peak shape of the broad peak suggested that this peak was composed of many peaks, we chose three fractions (8, 13, and 16) that corresponded with the broad peak and further analyzed these fractions in detail.

Fractionated Sample Analysis by Raman Spectrometry (RBM Region)

Nondestructive off-line analysis for fractionated samples is a useful technique for the detailed and precise characterization of samples, because off-line analytical method has almost no limitation in analytical time and technique. For on-line analysis, however, there are limitations in analytical time (sampling rate is usually 4 Hz in on-line CE) and

technique since sample does not stay the detection cell and pass the cell immediately. SWNTs have shown strong resonance Raman scattering signals, and the detection of single SWNTs by Raman spectrometry has been achieved by many researchers.^{38,39)} The signal in the radial breathing mode (RBM) region in Raman spectrometry corresponds to the vibration of carbon atoms in the radial direction of the SWNTs.⁷⁾ These features are unique to SWNTs and can be used to probe the chiral index of SWNTs. Thinner SWNTs show a larger Raman shift in the RBM region, whereas thicker SWNTs show a smaller Raman shift. A high-resolution spectrum is required for the assignment of the chiral index, because the Raman shifts of individual SWNTs in the RBM region are similar. For example, the Raman shifts of (10,3) and (11,1) SWNTs are 251 and 256 cm^{-1} , respectively, when a 633-nm laser is used. To obtain high-resolution spectra of the fractionated sample, the spectra were acquired for 10 seconds in each spot. The signal intensity of our method was improved by several tens of times higher than that of the equivalent on-line detection method, and it would be further improved with increasing acquisition time. We selected 768 spots (at 1.5- μm intervals) and collected a Raman spectrum at each spot with a resolution of 0.6 cm^{-1} . This resolution was sufficient to identify the chiral index of SWNTs with similar Raman shifts, such as (10,3) and (11,1) SWNTs. Fig. 3 shows 256 spectra of SWNTs that were measured in different spots in fraction 16. Raman signals in the RBM region are often broadened due to various factors, including SWNT bundling.^{38,39)} However, the halfwidth of each peak in the present spectra was very narrow (about 3.8 cm^{-1}), indicating that these detected peaks corresponded to isolated SWNTs. Most of the spectra featured no signal at all (upper spectra of Fig. 3), and some spectra featured scattering signals. Four peaks were

detected at 251, 256, 262, and 282 cm^{-1} in this RBM region, and these peaks were assigned as (10,3), (11,1), (7,6), and (7,5) SWNTs, respectively.^{40, 41)} These results indicate that SWNTs were located in only some of the areas on the glass plate that were analyzed.

Distribution of SWNTs in a Fraction

We converted the spectra of the four types of SWNTs that exhibited signals in the RBM region to a distribution image (Fig. 4). The size of the image was 24 μm x 24 μm , and we divided the image into 256 spots. Each spot was numbered as shown in Fig. 4, and the spots that exhibited Raman signals were labeled with different colors. SWNTs of (10,3), (11,1), (7,6), and (7,5) were labeled by red, purple, pink, and yellow, respectively. As mentioned previously and as reflected by the distribution image, SWNTs were present only in some places on the glass slide. Furthermore, only one spot (184) contained two types of SWNTs ((10,3) and (7,6)). Most of the spots in Fig. 4 are white, indicating that no scattering signal was obtained in the RBM region for these spots. The distribution image also indicates that most of the Raman signals were derived from single SWNTs, both because the distribution of SWNTs among the image spots was random and because very few signals were observed in the image. Even though we are observing only certain SWNTs which are resonant with 633 nm laser, they are isolated SWNTs at least in spectroscopic sense. Some adjoined spots, including spots 92 and 93 and spots 147 and 163, produced signals at the same wavelength. We expected that these signals were caused by single SWNTs that occupied both spots. These results show that CE-Raman spectrometry is a powerful analytical system for separation and detection of SWNTs and that this method

can be used to identify the chiral index of single SWNTs.

Comparison of Fractions by Raman Spectrometry (RBM Region)

We compared the peak intensities of the four types of SWNTs, that is (10,3), (11,1), (7,6), and (7,5) SWNTs, among three fractions (fractions 8, 13, and 16). Fig. 5a shows the spectrum of each fraction; each spectrum averaged 768 spectra. The intensities of the peaks at 283 and 251 cm^{-1} were similar to the peak intensities observed in the SWNT solution before CE separation. Although the ratio of these two peaks was not changed in fraction 13 relative to those in the unseparated SWNT solution, the (10,3) peak decreased in fraction 8 and increased in fraction 16. Notably, the diameters of (7,6), (11,1), and (10,3) SWNTs were 0.90, 0.92, and 0.94, respectively; their diameters are different in the range of 0.02 nm. Fig. 5b shows the peak area ratios (relative to the (7,5) peak) of three types of SWNTs for each of these three fractions. The maximum peak area ratios differed among the three SWNTs. For example, the maximum for the (7,6) SWNTs was observed in fractions 8 and 13, that of (11,1) was observed in fraction 13, and that of (10,3) was observed in fraction 16 (or possibly later, since the (10,3) peak area ratio appeared to still be increasing at fraction 16). Although the signal intensity of SWNTs is susceptible to their existing environment, we tried to reduce those influences by measuring many spectra of isolated SWNTs. The different peak top of the each SWNT in the separated three fractions may be driven by the diameter-different recognition. These results may indicate that the thicker SWNTs, i.e., the (10,3) SWNTs, migrated later than did the thinner (7,5) SWNTs during CE, and it thus we expected that the CE separation was based on the diameter of SWNTs. We hypothesis that

the separation of SWNTs based on their diameter difference occurred by the difference of the electric density of the complex of SWNTs and dispersant. It was reported that the number of dispersant interacting with SWNTs was changed by the diameter of SWNTs and it changed the properties of the complex.^{42, 43)}

Observation of a Fractionated SWNT by SPM

Finally, the fractionated sample was observed by SPM, which is a suitable analytical tool for the observation of nanomaterial structures owing to this tool's high resolution (less than 1 nm). However, there have been no reported studies that use CE-SPM techniques. There are two difficulties associated with the coupling of these two techniques. One difficulty is that SPM cannot be used to analyze compounds that are in motion in solution, and the other is that long analysis times are required to achieve high-resolution imaging. For example, analysis of a square space of 5 μm x 5 μm with 1 nm resolution requires about 10 minutes. For CE-SPM analysis, we fractionated the separated sample on the coated glass plate. The separated peaks by CE were collected at each spot for 12 seconds.

We expected that only SWNTs and the dispersant would be observed in SPM, because a volatile salt (ammonium acetate) was used as the electrolyte in this study. Fig. 6 shows an error signal image of fraction 16. The large round shape structures were expected to be derived from the presence of dispersant. A clear image of a fibrous structure with a height of about 1 nm is observed. On the basis of spectroscopy studies, we recently proposed that the SWNTs were wrapped with dispersant.³⁷⁾ These results indicate that this

fibrous structure was the image of an individual SWNT wrapped with dispersant and not of bundled SWNTs, since only one SWNT was observed in this 2- μm square space. These fibrous structures were observed in fractions that were detected G-band by Raman spectrometry. Therefore, CE-SPM also was a useful tool for the analysis of SWNTs.

Conclusions

We developed an analytical system that couples a high-efficiency separation technique with a highly sensitive detection technique. This combination of techniques was further enhanced by the use of an accurate fractionation system that enabled the enrichment of fractionated samples. This enrichment enabled the easy, efficient detection and characterization of fractionated SWNTs. This is the first time to fractionate SWNTs by means of CE and to characterize their structure precisely by means of Raman spectrometry and SPM. The developed CE-Raman spectrometry and CE-SPM systems are powerful tools for the analysis of SWNTs. We expect that these systems could be applied to other nanomaterials, such as β -amyloid and quantum dots, because the systems can be used to separate and characterize nanomaterials precisely.

Acknowledgments

This work was supported by a grant from the Ministry of Education, Culture, Sports, Science and Technology of Japan, and New Energy and Industrial Technology Development Organization. The authors acknowledge Dr. Yasushi Nakata (HORIBA Jobin Yvon) and Prof. Suguru Noda (Univ. Tokyo) for use of the Raman spectrometry, Prof. Jun

Miyake (AIST and Univ. Tokyo) for use of the NanoWizard and Dr. Robert H. Hauge (Rice University) for kindly supplying purified HiPco SWNTs.

REFERENCES

- (1) Zhang, L. J.; Webster, T.J. *Nano Today* 2009, 4, 66-80.
- (2) Warheit, D. B.; Sayes, C. M.; Reed, K. L.; Swain, K. A. *Pharmacology & Therapeutics* 2008, 120, 35-42.
- (3) Bruchez, M.; Moronne, M.; Gin, P.; Weiss, S.; Alivisatos, A. P. *Science* 1998, 281, 2013-2016.
- (4) Chan, W. C. W.; Nie, S. M. *Science*, 1998, 281, 2016-2018.
- (5) Silva, G. W. C.; Ma, L. Z.; Hemmers, O.; Lindle, D. *Micron*, 2008, 39, 269-274.
- (6) Misewich, J. A.; Martel, R.; Avouris, P.; Tsang, J. C.; Heinze, S.; Tersoff, J. *Science* 2003, 300, 783-786.
- (7) Kavan, L.; Dunsch, L. *ChemPhysChem*. 2007, 8, 975-998.
- (8) Shapiro, I. R.; Solares, S. D.; Esplandiú, M. J.; Wade, L. A.; Goddard, W. A.; Collier, C. P. J. *Phys. Chem. B* 2004, 108, 13613-13618.
- (9) Kato, M.; Sakai-Kato, K.; Matsumoto, N.; Toyo'oka, T. *Anal. Chem.* 2002, 74, 1915-1921.
- (10) Sakai-Kato, K.; Kato, M.; Toyo'oka, T. *Anal. Chem.* 2002, 74, 2943-2949.
- (11) Kato, M.; Sakai-Kato, K.; Jin, H.-M.; Kubota, K.; Miyano, H.; Toyo'oka, T.; Dulay, M. T.; Zare, R. N. *Anal. Chem.* 2004, 76, 1896-1902.
- (12) Swinney, K.; Bornhop, D. J. *Electrophoresis* 2000, 21, 1239-1250.
- (13) Ludwiczak, P.; Brando, T.; Monsarrat, B.; Puzo, G. *Anal. Chem.* 2001, 73, 2323-2330.
- (14) Amini, A.; Olofsson, I.-M. *J. Sep. Sci.* 2004, 27, 675-685.

- (15) Snovida, S. I.; Chen, V. C.; Krokhin, O.; Perreault, H. *Anal. Chem.* 2006, 78, 6556–6563.
- (16) Zuberovic, A.; Ullsten, S.; Hellman, U.; Markides, K. E.; Bergquist, J. *Rapid Commun. Mass Spectrom.* 2004, 18, 2946–2952.
- (17) Castoro, J. A.; Chiu, R. W.; Monnig, C. A.; Wilkins, C. L. *J. Am. Chem. Soc.* 1992, 114, 1511–1572.
- (18) Weinmann, W.; Parker, C. E.; Deterding, L. J.; Papac, D. I.; Hoyes, J.; Przybylski, M.; Tomer, K. B. *J. Chromatogr., A* 1994, 680, 353–361.
- (19) Muller, O.; Foret, F.; Karger, B. L. *Anal. Chem.* 1995, 67, 2974–2980.
- (20) Zhang, J.; Hu, H.; Gao, M.; Yang, P.; Zhang, X. *Electrophoresis* 2004, 25, 2374–2383.
- (21) Amon, S.; Plematl, A.; Rizzi, A. *Electrophoresis* 2006, 27, 1209–1219.
- (22) Johnson, T.; Bergquist, J.; Ekman, R.; Nordhoff, E.; Schurenberg, M.; Kloppel, K.-D.; Muller, M.; Lehrach, H.; Gobom, J. *Anal. Chem.* 2001, 73, 1670–1675.
- (23) Adams, M. D.; Kelley, J. M.; Gocayne, J. D.; Dubnick, M.; Polymeropoulos, M. H.; Xlao, H.; Merrill, C. R.; Ww, A.; Olde, B.; Moreno, R. F.; Kerlavage, A. R.; McCombie, W. R.; Venter, J. C. *Science* 1991, 252, 1651–1656.
- (24) Kambara, H.; Takahashi, S. *Nature*, 1993, 361, 565–566.
- (25) Kato, M.; Kinoshita, H.; Enokita, M.; Hori, Y.; Hashimoto, T.; Iwatsubo, T.; Toyo'oka, T. *Anal. Chem.* 2007, 79, 4887–4891.
- (26) Ban, T.; Hoshino, M.; Takahashi, S.; Hamada, D.; Hasegawa, K.; Naiki, H.; Goto, Y. *J. Mol. Biol.* 2004, 344, 757–767.

- (27) Barone, P. W.; Baik, S.; Heller, D. A.; Strano, M. S. *Nat. Mater.* 2005, 4, 86-92.
- (28) Cherukuri, P.; Bachilo, S.M.; Litovsky, S.H.; Weisman, R.B. *J. Am. Chem. Soc.* 2004, 126, 15638-15639.
- (29) Jorio, A.; Dresselhaus, M. S.; Dresselhaus (Ed.), G.; *Topics in Applied Physics*, 111: Carbon Nanotubes, Advanced Topics in the Synthesis, Structure, Properties and Applications, Springer-Verlag: Berlin Heidelberg, 2008
- (30) Doorn, S. K.; Fields, R. E., III; Hu, H.; Hamon, M. A.; Haddon, R. C.; Selegue, J. P.; Majidi, V. J. *Am. Chem. Soc.* 2002, 124, 3169-3174.
- (31) Doorn, S. K.; Strano, M. S.; O'Connell, M. J.; Haroz, E. H.; Rialon, K. L.; Hauge, R. H.; Smalley, R.E. *J. Phys. Chem. B* 2003, 107, 6063-6069.
- (32) Suarez, B.; Simonet, B. M.; Cardenas, S.; Valcarcel, M.; *J. Chromatogr. A* 2006, 1128, 282-289.
- (33) Lopez-Pastor, M.; Dominguez-Vidal, A.; Ayora-Canada, M. J.; Simonet, B. M.; Lendl, B.; Valcarcel, M. *Anal. Chem.* 2008, 80, 2672-2679.
- (34) Murakami, Y.; Lu, B.; Kazaoui, S.; Minami, N.; Okubo, T.; Maruyama, S. *Phys. Rev. B*, 2009, 79, 195407.
- (35) Nish, A.; Hwang, J.-Y.; Doig, J.; Nicholas R. J.; *Nat. Nanotechnol.* 2007, 2, 640-646.
- (36) Yamamoto, T.; Miyauchi, Y.; Motoyanagi, J.; Fukushima, T.; Aida, T.; Kato, M.; Maruyama, S. *Jap. J. Appl. Phys.* 2008, 47, 2000-2004.
- (37) Yamamoto, T.; Motoyanagi, J.; Murakami, Y.; Miyauchi, Y.; Maruyama, S.; Kato, M. *Applied Physics Express*, 2009, 2, 055501.

- (38) Jorio, A.; Fantini, C.; Dantas, M. S. S.; Pimenta, M. A.; Souza, A. G.; Samsonidze, G. G.; Brar, V. W.; Dresselhaus, G.; Dresselhaus, M. S.; Swan, A. K.; Unlu, M. S.; Goldberg, B. B.; Saito, R. *Phys. Rev. B*, 2002, 66, 115411.
- (39) Fantini, C.; Jorio, A.; Souza, M.; Strano, M. S.; Dresselhaus, M. S.; Pimenta, M. A. *Phys. Rev. Lett.*, 2004, 93, 147406.
- (40) Kataura, H.; Kumazawa, Y.; Maniwa, Y.; Umezu, I.; Suzuki, S.; Ohtsuka, Y.; Achiba, Y. *Synth. Metals*, 1999, 103, 2555-25.
- (41) Bachilo, S. M.; Strano, M. S.; Kittrell, C.; Hauge, R. H.; Smalley, R. E.; Weisman, R. B. *Science*, 2002, 298, 2361-2366.
- (42) Arnold, M. S.; Green, A. A.; Hulvat, J. F.; Stupp, S. I.; Hersam, M. C. *Nature Nanotech.* 2006, 1, 60 – 65.
- (43) Arnold, M. S.; Stupp, S. I.; Hersam, M. C. *Nano Lett.* 2005, 5, 713-718.

Figure Captions

Fig. 1 a) Photograph of fraction plate, b) side view of outlet end of capillary and fraction plate, and c) schematic image of the end of capillary.

The black layer on the fraction plate is the hydrophobic coating, and the 1-mm clear circles are hydrophilic spots.

Fig. 2 Electropherograms of SWNT separation using CE.

Conditions: column, 100 cm fused silica capillary (100 μm i.d.); electrolyte, 100 mM Gly-NaOH buffer (pH 9). samples: a) and c) SWNT with dispersant; b) dispersant only. Means of detection: a), b) and dotted line in c) UV at 280 nm, solid line in c) Raman spectrometry at 1590 cm^{-1} .

Fig. 3 256 Raman spectra acquired for the RBM region of fraction 16 for a sample of SWNTs in dispersant.

Conditions: light source, He-Ne laser at 633 nm; resolution: 0.6 cm^{-1} ; accumulation time: 10 s.

Fig. 4 Distribution image of fraction 16.

Conditions are as described in Figure 3.

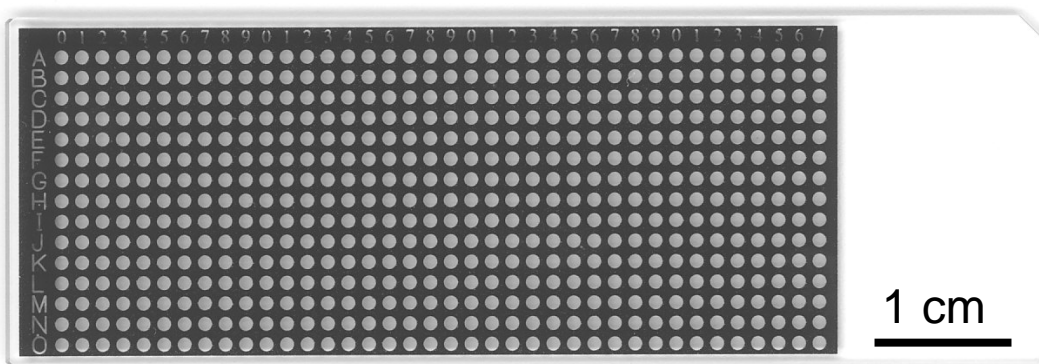
Fig. 5 a) Spectra and b) peak area ratio (relative to the (7,5) SWNT peak) of collected fractions.

The symbols •, •, and • indicate (10,3), (11,1), and (7,6) SWNTs, respectively.

Fig. 6 a) Error signal image of fraction 16 and b) cross-sectional topological profile of the image obtained along the white line drawn in a).

Supporting Fig. 1 Movie of the fractionation (eight-times speed than original one).

a)



b)

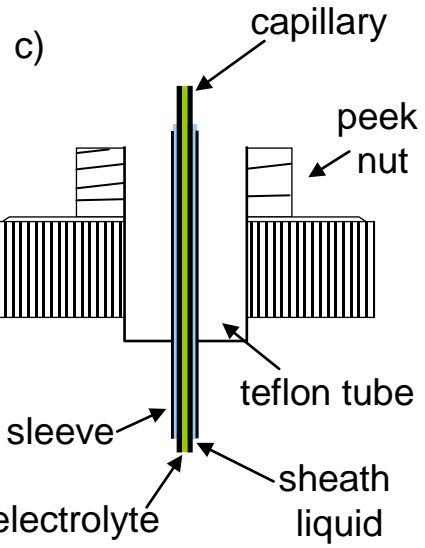
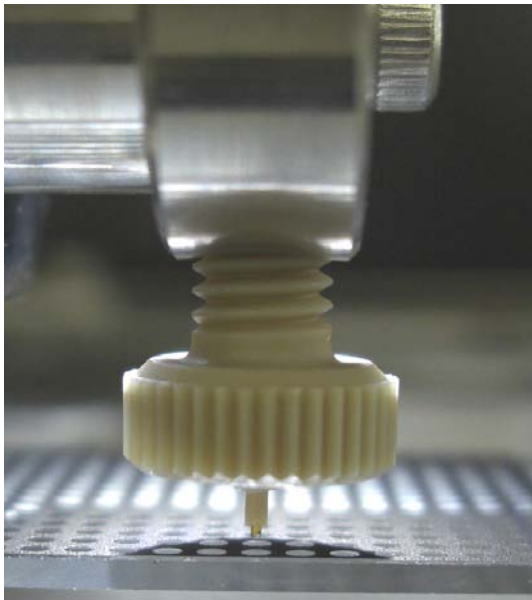


Fig. 1

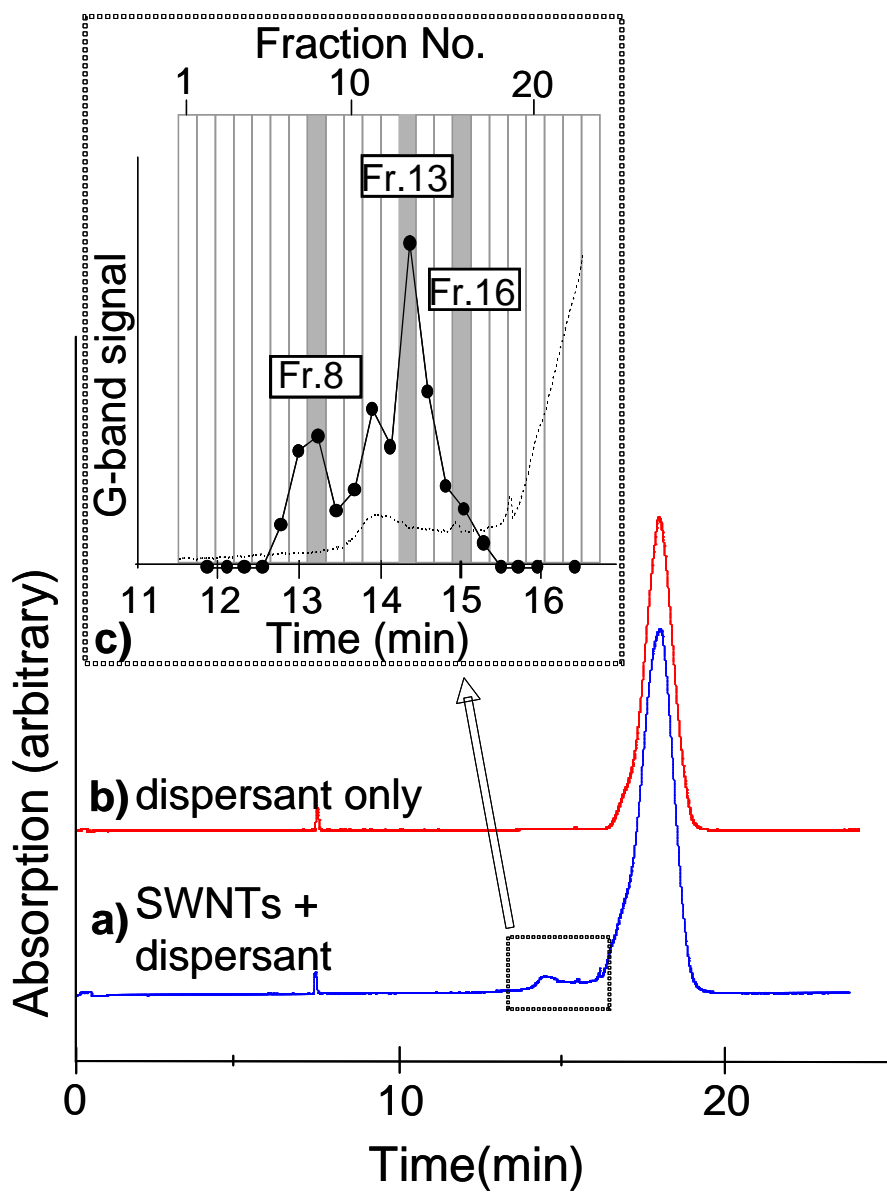


Fig. 2

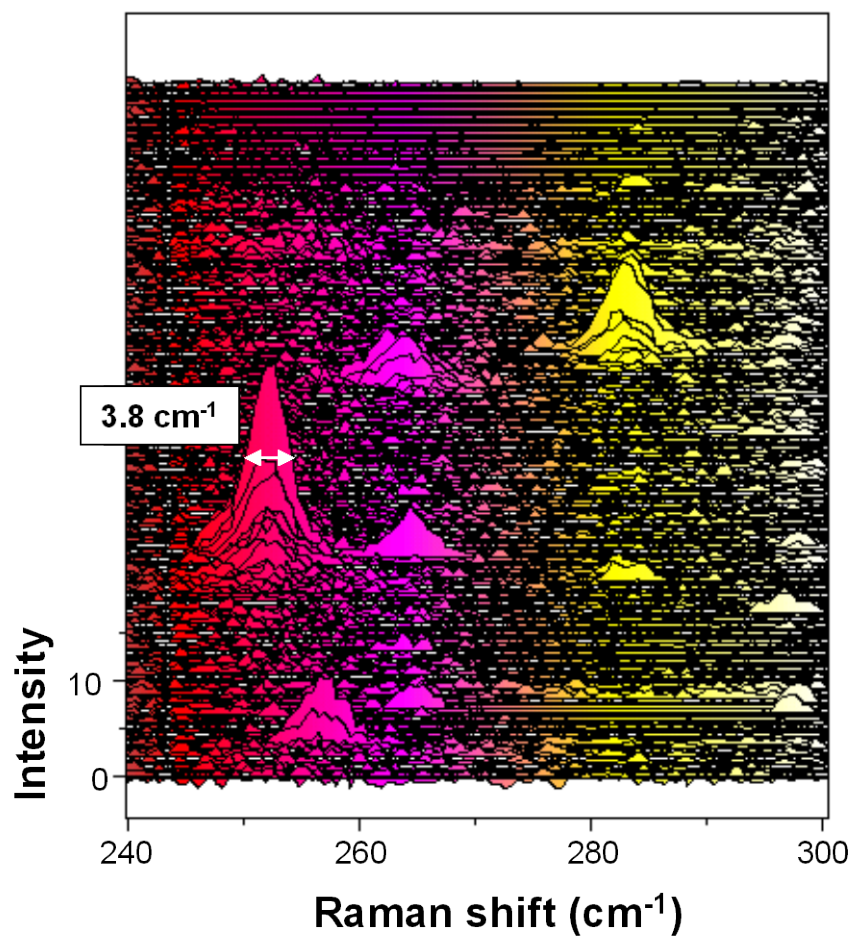


Fig. 3

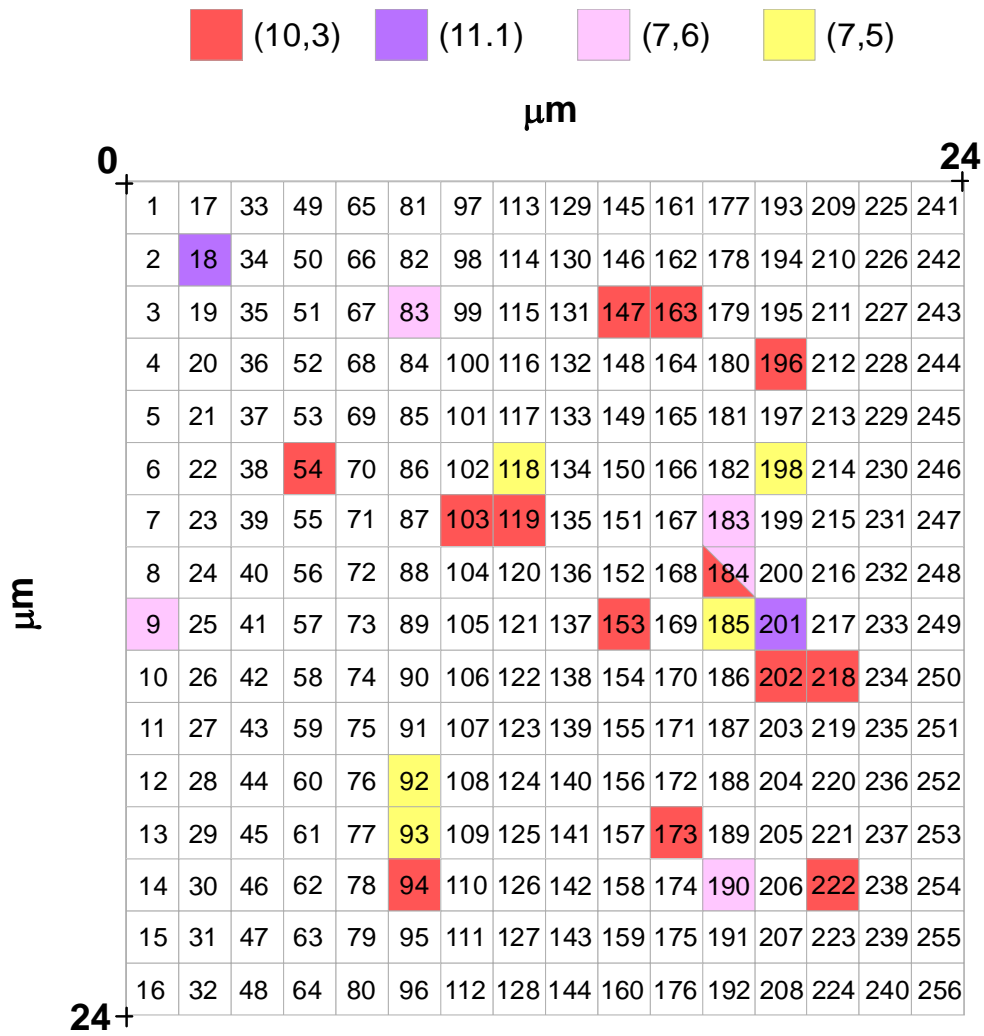


Fig. 4

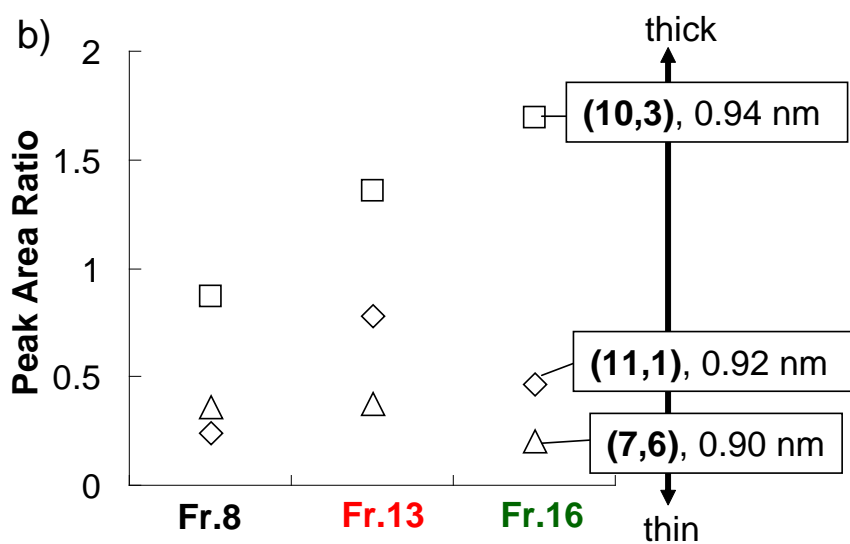
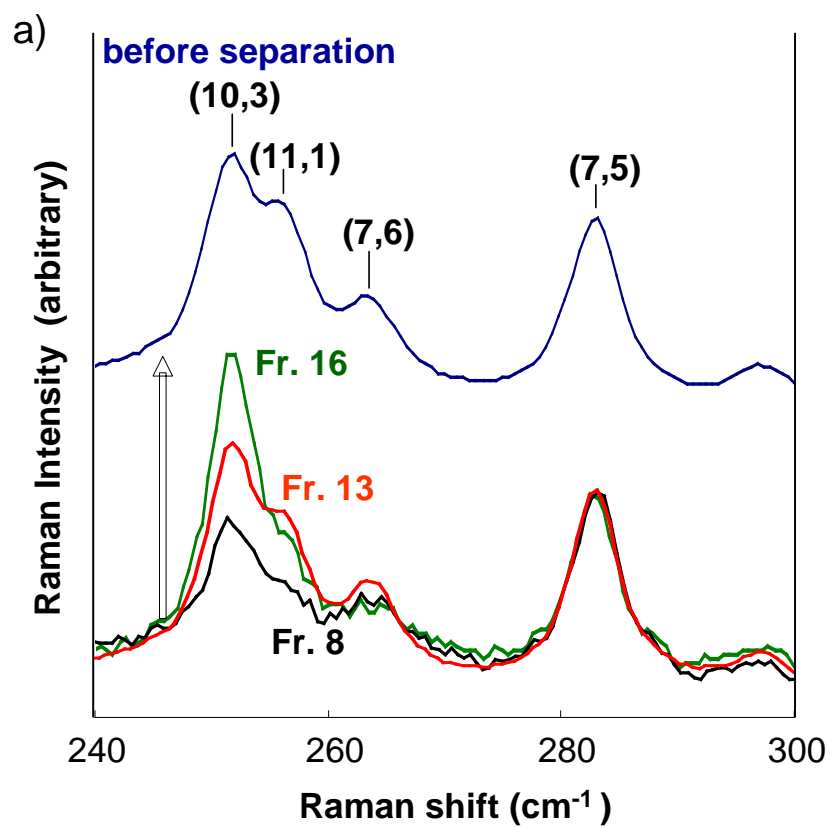
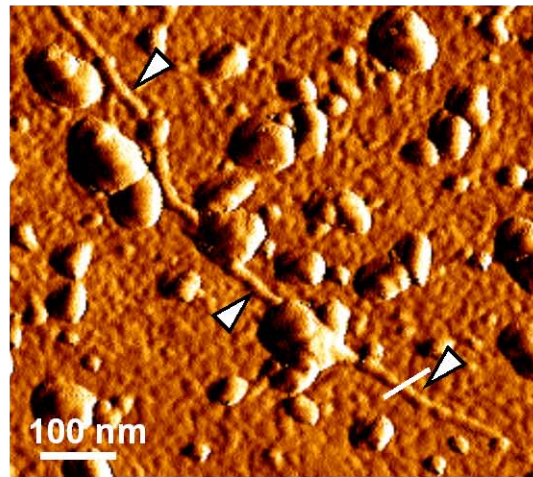


Fig. 5

a)



b)

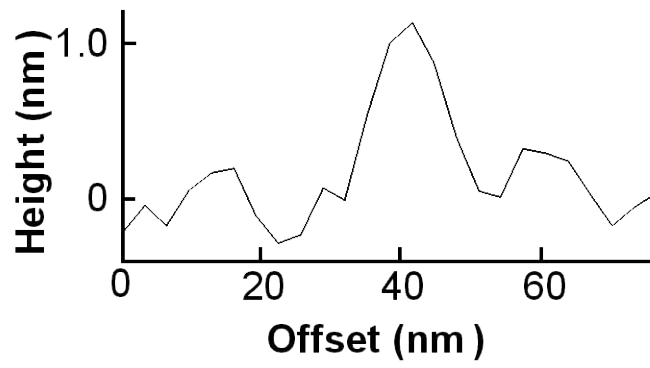


Fig. 6